

Evaluation of Infection Probability of Covid-19 in Different Types of Airliner Cabins

Feng Wang^{1,2}, Tengfei (Tim) Zhang^{1,3}, Ruoyu You^{2*}, and Qingyan Chen²

¹ Tianjin Laboratory of Indoor Air Environmental Quality Control, School of Environmental Science and Engineering, Tianjin University, Tianjin, China

²Department of Building Environment and Energy Engineering, The Hong Kong Polytechnic University, Hung Hom, Hong Kong

³ School of Civil Engineering, Dalian University of Technology, Dalian, China

**Corresponding email: ruoyu.you@polyu.edu.hk*

Highlights

1. Proposed a CFD based method to study airborne infectious diseases in an air cabin
2. Validated the CFD results by experimental data obtained from a cabin mockup
3. Evaluated infection probabilities in different airplanes and seats to COVID-19
4. Found flight time is the most important factor in the infection probability

Abstract

According to the World Health Organization (<https://covid19.who.int/>), more than 651 million people have been infected by COVID-19, and more than 6.6 million of them have died. COVID-19 has spread to almost every country in the world because of air travel. Cases of COVID-19 transmission from an index patient to fellow passengers in commercial airplanes have been widely reported. This investigation used computational fluid dynamics (CFD) to simulate airflow and COVID-19 virus (SARS-CoV-2) transport in a variety of airliner cabins. The cabins studied were economy-class with 2-2, 3-3, 2-3-2, and 3-3-3 seat configurations, respectively. The CFD results were validated by using experimental data from a seven-row cabin mockup with a 3-3 seat configuration. This study used the Wells-Riley model to estimate the probability of infection with SARS-CoV-2. The results show that CFD can predict airflow and virus transmission with acceptable accuracy. With an assumed a flight time of four hours, the infection probability was almost the same among the different cabins, except that the 3-3-3 configuration had a lower risk because of its airflow pattern. Flying time was the most important parameter for causing the infection, while cabin type also played a role. Without mask wearing by the passengers and the index patient, the infection probability could be 8% for a 10-hour, long-haul flight, such as a twin-aisle air cabin with 3-3-3 seat configuration.

Keywords: Air distribution, Computational fluid dynamics (CFD), Economy-class cabin, Experimental validation, Infectious disease, Wells-Riley model.

1. Introduction

Since the identification of the first COVID-19 case in Wuhan, China, in December 2019, the World Health Organization (<https://covid19.who.int/>) has reported that more than 651 million people have been infected, and more than 6.6 million of them have died. COVID-19 has spread to almost all the countries in the world because of air travel. Bae et al. [1], Hoehl et al. [2], Toyokawa et al. [3], and Swadi et al. [4] have reported cases of airborne transmission in the air cabins of commercial airplanes. Furthermore, Wang et al. [5], conducted a review of COVID-19 transmission cases in commercial airplanes. They found that the literature had documented cases of airborne transmission of the COVID-19 virus (SARS-CoV-2) in airliner cabins, although airplane manufacturers seemed to downplay the significance. In April 2020, airlines experienced a 94% reduction in passenger capacity worldwide due to the COVID-19 pandemic [6]. The flying public is greatly concerned about their health in the midst of this pandemic. Moreover, such a pandemic could seriously damage the aviation industry and the world economy. Other infectious diseases, such as measles [7] and tuberculosis [8], have been proven to be airborne. Airborne infectious diseases appear every few years. However, the air cabin environment cannot prevent airborne infectious disease transmission among passengers and crew members.

During the pandemic, health authorities such as the World Health Organization [9] and the U.S. Centers for Disease Control and Prevention [10] recommended social distancing as one of the most important safety procedures for reducing COVID-19 transmissions. Unfortunately, this is not always possible in commercial airplanes. Even in the business-class cabin of a long-haul, trans-continental flight, Khanh et al. [11] identified a cluster of COVID-19 infections. Commercial airplanes rely on HEPA filters to remove airborne infectious viruses. However, virus transmission could occur before the air containing the virus has been recirculated through the HEPA filters. High passenger density, especially in economy-class cabins, can easily lead to the spread of respiratory diseases [12].

At the same time, air cabins use mixing ventilation systems that are intended to mix supply air with cabin air to create a uniform air temperature for thermal comfort, as reviewed by Wang et al. [5]. However, the mixing system makes it difficult to remove airborne viruses. Mizuno and Warfield [13] found that CO₂ distribution in a twin-aisle cabin was not uniform. Lin et al. [14] simulated measles-laden aerosol transport in a twin-aisle cabin and found that the aerosols were mainly in the vicinity of the source. Similarly, Kinahan et al. [15] found that the exposure risk depended on the specific seat location by using fluorescent tracer and DNA-tagged measurement methods in B767 and B777 twin-aisle cabins. Yan et al. [16] conducted experimental tests and computer simulations in a five-row, twin-aisle cabin mockup. An airborne pollutant was released and spread mainly on the same side of cabin as the source; it spread very little to the other side of the cabin, because the airflow pattern was observed to be symmetric in the middle of a cabin section. Studies by You et al. [17] and Cao et al. [18] also found that the fine particles generated by a passenger in a single-aisle cabin with a mixing ventilation system would not be easily transferred to the other side of the aisle. Yan et al. [19] studied a cough by a passenger in a single-aisle cabin. The contaminant generated by the cough could remain locked in near and intermediate fields around passengers. Thus, the resident time

of the contaminant in the cabin depended very much on the source location. You et al. [20] evaluated the SARS infection risk caused by an index person in different seats of single-aisle and twin-aisle airplanes. They concluded that the risk differed greatly, even under mixing ventilation systems. The above literature shows that infection risk depends on airplane type and seat location.

Significant efforts have been made in evaluating the infection risk of airborne diseases in commercial airplanes. An early study by Mangili and Gendreau [12] found that the perceived risk was greater than the actual risk, and the authors believed that the environmental control system could limit the spread of a virus. However, actual data collected by Hertzberg and Weiss [21] provided strong evidence of in-flight infection. They also found that most infections occurred in close proximity to the infector. Gupta et al. [22] studied influenza infection during a four-hour flight and concluded that both deterministic approaches using inhaled influenza virus RNA particles and a probabilistic approach employing the Wells-Riley model could be used. A deterministic approach utilizing inhaled viral copies can accurately estimate COVID-19 infection in airliner cabins [23]. Horstman and Rahai [24] used the Wells-Riley model to assess the COVID-19 infection risk in a Boeing-737 airplane. During a three-hour flight, the risk of infection was nearly 50% for those sitting in the vicinity of the infector. The use of the Wells-Riley model was more popular than the deterministic approach, such as by Yin, et al. [25], Yan et al. [26] and Liu et al. [27].

The above literature review concluded that the risk of airborne infectious disease transmission in commercial airliner cabins is high. Social distancing is impossible in the cabins and filters could not remove the virus transmission in the cabins before entering the environmental systems. The virus distribution in a cabin is not uniform even under a mixing ventilation system. The probabilistic model with the Wells-Riley equation could be a good method to evaluation the infection probability. But, there are no systematic studies to compare infection risk in different types of airliner cabins. Therefore, the present study tried to compare the infection probability of COVID-19 in commercial airplanes of different sizes, including those with 2-2, 3-3, 2-3-2, and 3-3-3 seat configurations, which represents popular single-aisle and twin-aisle air cabins. The Wells-Riley model was used to calculate the infection risk during a four-hour flight, and for different flight times with different types of aircraft cabins.

2. Research Method

2.1 Airflow simulation

Modern commercial aircraft cabins have been designed to minimize airflow along the longitudinal direction. On a cross section, the airflow is symmetric. Since airborne infectious disease viruses such as SARS-CoV-2 are transferred with airflow, the airflow pattern plays a very important role in virus transmission.

Liu et al. [28] conducted a comprehensive review of research methods for studying airflow and airborne contaminant transmission in commercial airplane cabins. They concluded that both experimental measurements and numerical simulations were popular research methods. Although the experimental measurements were reliable, they were expensive and time

consuming. Numerical simulations by computational fluid dynamics (CFD) can provide detailed information. Due to the many assumptions used in the CFD simulations, validation of the CFD results with experimental data is necessary. Among numerous CFD models, the re-normalization group (RNG) k- ϵ model [29] is the best choice at present for balancing accuracy and the need for computing resources. Other models, such as SST k- ω model may perform well in some cases, but it is less stable than the RNG k- ϵ model [30]. Therefore, this study used the RNG k- ϵ model to simulate airflow, contaminant transport, and air temperature distributions in various types of commercial airliner cabins.

The RNG k- ϵ model is a turbulence model based on Reynolds-averaged Navier-Stokes equations. The entire set of governing equations can be written as

$$\frac{\partial(\rho\Phi)}{\partial t} + \text{div}(\rho\vec{u}\Phi - \Gamma_{\phi,eff}\text{grad}(\Phi)) = S_{\Phi} \quad (1)$$

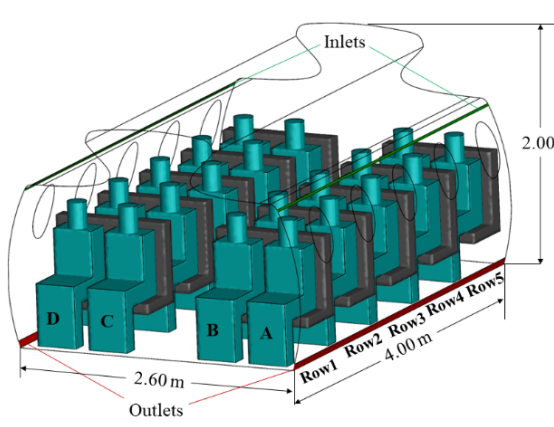
where ρ is air density; Φ represents the time-averaged velocity components \vec{u}_i ($i = 1, 2, 3$), turbulent kinetic energy k , dissipation rate of turbulent kinetic energy ϵ , enthalpy H , and contaminant concentration C ; the t is time; \vec{u} is the Reynolds-averaged air velocity vector; $\Gamma_{\phi,eff}$ is the diffusion coefficient; and S_{Φ} is a source term. When Φ is unity, the equation becomes the continuity equation. Since temperature variation in an airliner cabin is rather small, this simulation assumed air density to be constant, and the buoyancy effect was considered with the Boussinesq approximation [31].

This investigation solved the governing transport equations numerically by the finite volume method. Fluent Meshing 19.2 software was used to generate grid cells for the cabin geometric model.

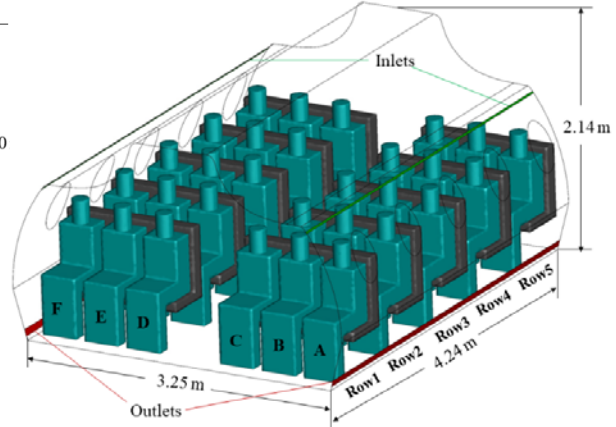
The numerical method used the semi-implicit method for pressure-linked equations (SIMPLE) algorithm for coupling pressure and velocity equations, and the second-order discretization schemes for the convection and viscous terms of the governing equations. A commercial CFD program, ANSYS Fluent [32], was utilized. When we use this program, we typically run each case for 25,000 iterations. The cases can be regarded as reached convergence with velocity residuals at 10^{-3} , turbulence residuals at 10^{-4} , and energy residuals at 10^{-6} .

Figure 1 shows four different cabins studied in this investigation with different seat configurations for economy class. The 2-2 seat configuration represents an airliner such as the Embraer 195. The 3-3 seat configuration simulates the Boeing 737 or Airbus 320. The 2-3-2 seat configuration is a mockup of the Boeing 767. The 3-3-3 seat configuration models the Boeing 777, Boeing 787, or Airbus 350. Please note that the simulated cabins were different from their real-life counterparts in terms of their geometry and thermo-fluid boundary conditions. We selected only a section of five rows in the economy-class cabins. Beneke et al. [33] measured the particles generated at the breathing level of a manikin in an 11-row B767 mockup. They found rapid drop-off in the particle concentration along the longitudinal direction. This drop-off occurred with a roughly 37% reduction in concentration with each successive row from the source. Hertzberg and Weiss [21] found that infection occurred mostly within two rows behind and two rows in front of an index patient. Similarly, Dietrich et al. [34] found that 75% of infected passengers were seated within two rows of the symptomatic

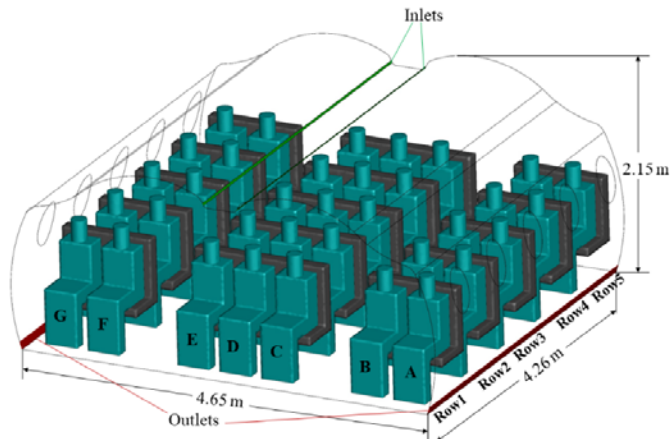
passenger. Therefore, this investigation used five-row cabin models, which should be sufficient. Early studies [28,35] in an actual MD-82 aircraft cabin have already confirmed that five rows were sufficient. To eliminate possible errors in the both ends by using solid walls, our study for the five-row cabin section used periodical boundary conditions.



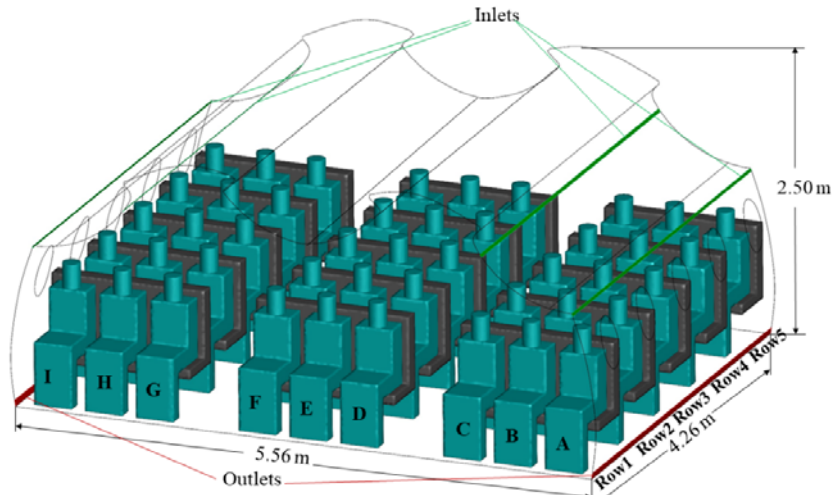
(a) 2-2 seat configuration



(b) 3-3 seat configuration



(c) 2-3-2 seat configuration



(d) 3-3-3 seat configuration

Figure 1. Computer models for cabins with different seat configurations.

Table 1 lists the thermal and fluid boundary conditions used in our simulations. The surface temperatures were averaged measured data in various commercial airlines. Since this study did not include the heat generated from electronics, the supply air temperatures were adjusted to keep energy conserved in the cabins. The total air supply rate was 10 L/s per passenger that was a typical design value. We also assumed that the cabins were fully occupied.

Table 1. Boundary conditions

Items	Settings
Cabin	Temperature 24 °C
Seats	Adiabatic
Occupant body	Temperature 29.5 °C
Occupant head	Temperature 30.5 °C
Luggage cabin wall	Temperature 24°C
Ceiling wall	Temperature 22.62 °C
Front and back surfaces	Symmetry
Floor	Temperature 24.5 °C
Window	Temperature 15 °C
Outlets	Outflow
Inlets	10 L/s per person 2-2 configuration, air temperature 21.2°C, air velocity 1.30 m/s 3-3 configuration, air temperature 20.7°C, air velocity 1.65 m/s 2-3-2 configuration, air temperature 21.4°C, air velocity 1.37 m/s 3-3-3 configuration, air temperature 21.8°C, up inlet air velocity 0.92 m/s and shoulder inlet air velocity 0.63 m/s.
SARS-CoV-2 source	20 quanta/h

2.2 Wells-Riley model

Wells [36] proposed the quantum of infection as a hypothetical infectious dose unit. A quantum is the number of infectious airborne particles required to infect a person. To evaluate the probability of infection, Riley [37] considered intake dose of airborne pathogens in terms of the number of quanta. The probability can be determined by the Wells-Riley equation:

$$P = 1 - e^{-Iqpt/Q} \quad (2)$$

where P is the infection probability for the susceptible person; I the number of index patients; q the quanta produced by each patient (h^{-1}); p the pulmonary ventilation rate of each susceptible person (m^3/h), in a seated position or doing light activity, $p = 0.3 \text{ m}^3/\text{h}$; t the duration of exposure (h); and Q the ventilation rate of clean air supplied to the five-row cabin (m^3/h). The quanta range for SARS-CoV-2 estimated by Dai and Zhao [38] was 14 quanta/h to 48 quanta/h, and the present investigation used 20 quanta/h. Note that the quanta number depends on toxicity

of virus. Even for COVID-19, Omicron virus had a much lower quanta value than early virus variants. This study used 20 quanta/h was for the virus transmission case used in this study. Assuming only one index patient in a cabin, Eq. (2) can be re-written as follows to calculate local infection probability:

$$P = 1 - \exp(-1 \times C \times 0.3 \text{ m}^3/\text{h} \times 4 \text{ h}) = 1 - \exp(-1.2C) \quad (3)$$

where C is the local quantum concentration (quanta/ m^3). Since the quantum distribution in a cabin is highly non-uniform, this study used the average concentration over a volume of $0.3 \text{ m} \times 0.3 \text{ m} \times 0.3 \text{ m}$ in front of a passenger's nose. In Eq. (3), quantum particle concentration is replaced by gaseous concentration. Li et al. [39] compared the measured concentration fields of SF_6 and the 3 mm particles in an air cabin. They found that the two distributions matched with each other well in the measured sections. For particles with a large diameter, they will fall into floor due to gravity and cannot be inhaled by a passenger. The study from Dai and Zhao [38] considered the quanta released to have no mass and with zero initial velocity.

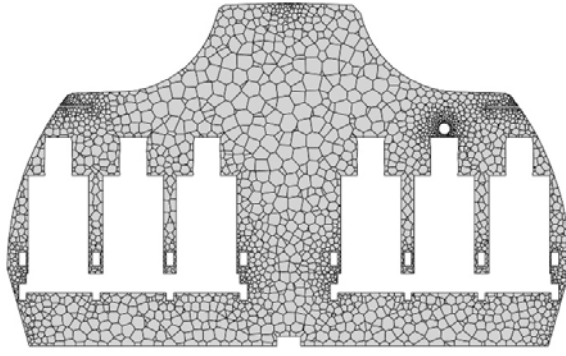
3. Validation of the CFD Simulations

Before we applied the CFD simulation tool to study the infectious disease transmission in an airliner cabin, this investigation carried out two very important steps to ensure the accuracy of the simulation results reported in this paper: a grid-independence study and experimental validation.

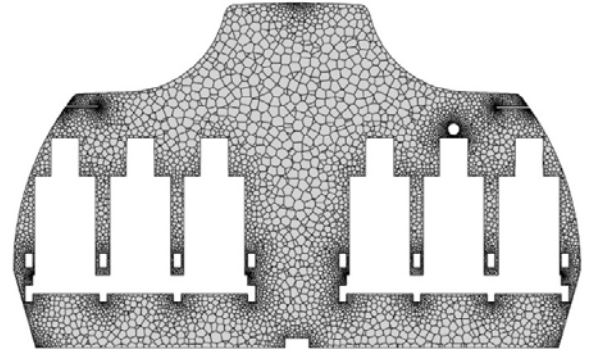
3.1 Grid-independence study of the CFD simulations

When one applies CFD to study airflow and contaminant dispersion in an airliner cabin, the grid resolution used should be sufficiently fine to obtain accurate results. If the grid is too coarse, the numerical diffusion caused by discretization of the Navier-Stokes equations would lead to significant errors. On the other hand, if the grid is too fine, the computing capacity required would be too large and the computing time would be too long for such a study, since even a section of an airliner cabin with several rows of seats is a very large space for CFD simulation.

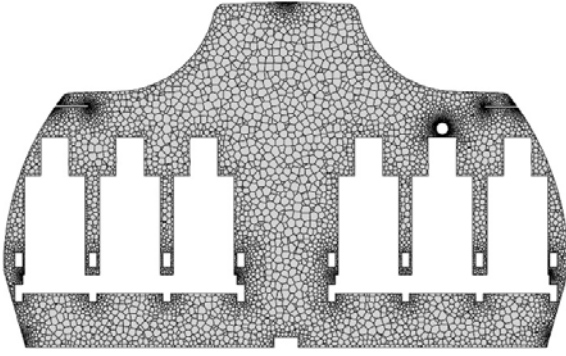
We used a seven-row cabin with 3-3 seat configuration [18] similar to the one shown in Figure 1(b) as an example to demonstrate the grid-independence study. Both ends of the cabin were solid walls as the experiment. Figures 2(a)-(c) show the three grids studied in a cross section through the middle row of seats in the cabin: a coarse grid of 0.96 million, a moderate grid of 2.92 million, and a fine grid of 4.12 million, respectively, for the seven-row cabin. The grid distribution was finer near the solid boundary layers and in the regions where velocity gradients were large. Since this study used enhanced wall functions for the boundary, very fine grids were used only in key regions where gradients were high, such as near the inlet and tracer-gas source. For other regions, minimal grids were used to reduce computing cost.



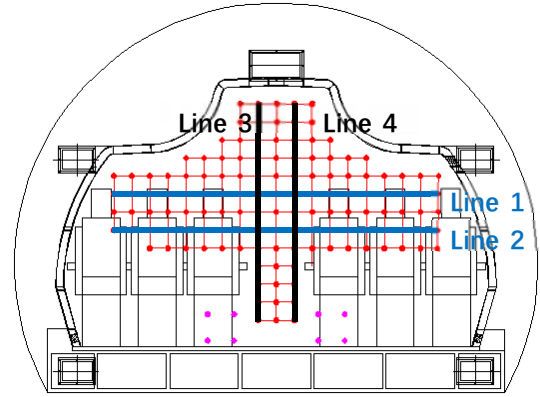
(a) With coarse grid of 0.96 million



(b) With moderate grid of 2.92 million



(c) With fine grid of 4.12 million



(d) Comparison made on lines 1-4

Figure 2. Grid distributions for the grid-independence study and the locations where the measured data and CFD simulation results were compared.

The circle above the middle passenger on the right side of the cabin was a sphere source for releasing tracer gas. The tracer gas was considered as a species and its concentration, C , was modeled by a transport equation (Eq. 1). Although the air velocity was measured at many points as shown in Figure 2(d), we have compared the CFD simulation results on four lines to save space in this paper.

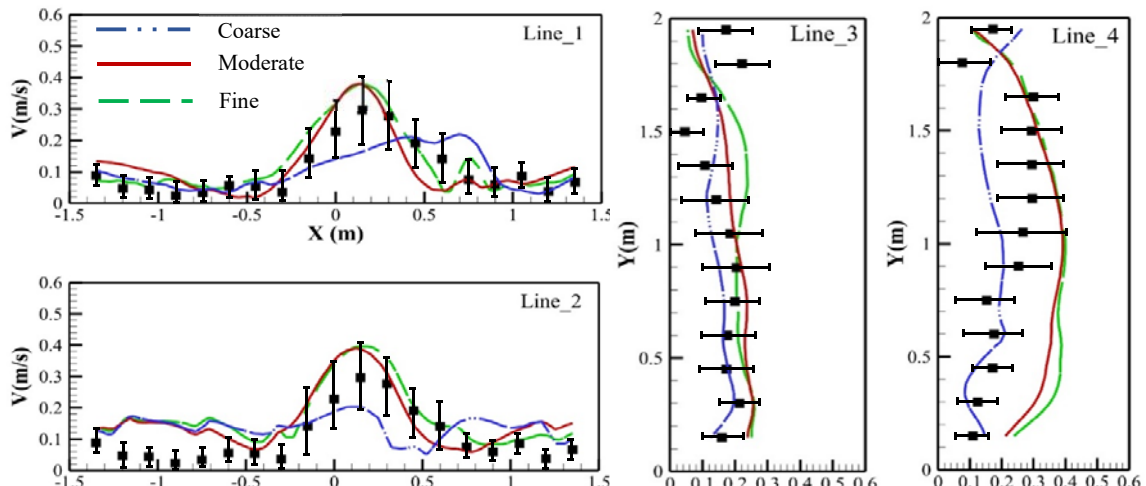


Figure 3. Comparison of the air velocity along the four lines obtained by CFD simulations with the three grids and the corresponding experimental data.

Figure 3 compares the air velocity along the four lines in the cabin cross section obtained by CFD simulations with the three grids, and the corresponding experimental data with error bars. Clearly, the CFD simulation with the coarse grid could not predict the air velocity accurately. The air velocities simulated with the moderate and fine grids were similar and also within the error bars at most of the data points. The disagreement between the simulated results and the experimental data can be attributed to many causes, such as complex geometry, unstable flow, instrument error, and uncertainties in the turbulence model and numerical algorithm. The results confirmed that the moderate grid provided a reasonably accurate prediction of the air velocity distribution. Further refinement of the grid may not lead to better accuracy. Therefore, the moderate grid was subsequently used to obtain the results presented in the following sections.

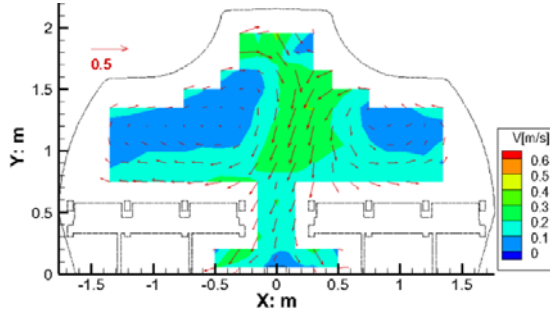
Note that this investigation studied different types of economy-class cabins as shown in Figure 1. We used similar grid resolutions for other cabins as the moderate grid used for the cabin with the 3-3 seat configuration. The grid numbers for the five-row cabin mockups were 1.85 million for the 2-2 seat configuration, 2.47 million for the 3-3 seat configuration, 2.90 million for the 2-3-2 seat configuration, and 3.14 million for the 3-3-3 seat configuration. The maximum size of the cells was 0.06 m. The variation in grid size between two neighboring cells was less than 1.15 times to reduce numerical diffusion.

3.2 Validation of major airflow parameters calculated by CFD

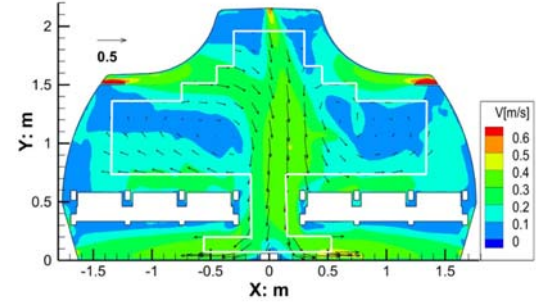
As mentioned briefly in the previous section, the development of the RNG $k-\epsilon$ model used many approximations to model the turbulence parameters. The discretization scheme and numerical procedure also introduced errors to the simulations. A CFD user has to make numerous assumptions in order to simulate airflow in a cabin. Therefore, the CFD results cannot be trusted unless the results are validated, thus confirming that CFD can be used to conduct such simulations accurately [40].

This investigation used experimental data from Cao et al. [18] for validating the CFD model. The experimental measurements were conducted in a seven-row cabin mockup with a 3-3 seat configuration similar to that shown in Fig. 1(c). The experiment measured the airflow pattern, air temperature, and tracer-gas concentration simulated by a mixture of 1% sulfur hexafluoride (SF_6) and 99% of nitrogen. The SF_6 was released at steady rate above the head of the middle passenger on the right side of the cabin.

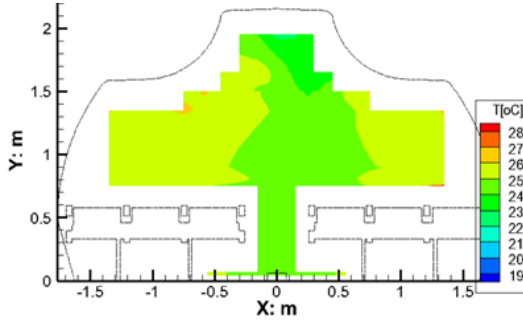
Figure 4 compares the air velocity, air temperature, and tracer-gas concentration distributions in the cross-section through the fourth row simulated by CFD with the corresponding measured distributions. Both the simulated and measured airflow patterns show two large recirculation patterns in the cross section, but the airflow direction deviated slightly in the aisle. However, the air velocity magnitude was similar between simulation and measurement. Figures 4(c) and (d) show a well-mixed air temperature. The air temperature difference in the measured region was less than 2 K and was reproduced well by the simulation. However, the simulated air temperature distribution was less uniform than the measured one. The most significant discrepancy was in the SF₆ distributions in which the experiment showed stronger dispersion of SF₆ from the right side of the cabin to the left side. In contrast, the simulation shows almost no dispersion from the right side of the cabin to the left side. Many past studies, such as Li et al. [41] and Guevara et al. [42], found that it was difficult to simulate SF₆ distributions accurately in confined indoor spaces. The equipment used to measure SF₆ is based on photoacoustic technique. It took about 30 s to measure the SF₆ concentration at a location. On the other hand, airflow in a cabin was not very stable, the airflow pattern could have changed a lot in 30 s. Nevertheless, the simulation did predict the peak SF₆ location. The accuracy was not ideal, but it was acceptable for the present applications. Our results are comparable to other studies [43-45]. Therefore, we considered that the CFD results were validated, and the CFD tool could then be used for the proposed evaluation of COVID infection risk in different types of airliner cabin environment.



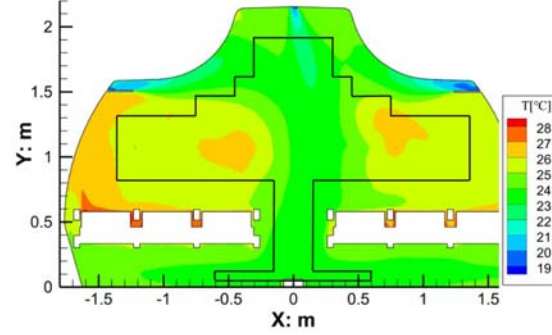
(a) Measured air velocity



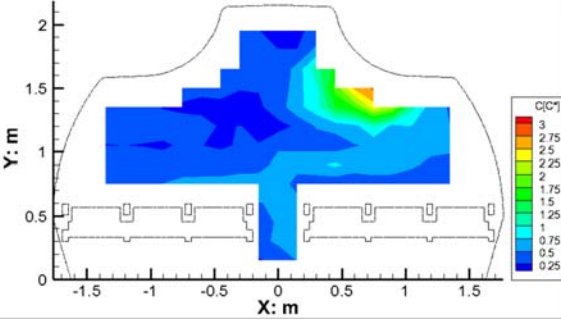
(b) Simulated air velocity



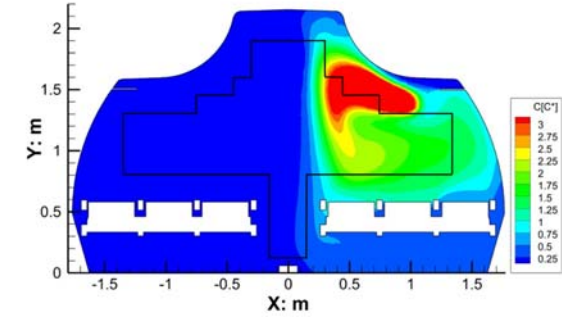
(c) Measured air temperature



(d) Simulated air temperature



(e) Measured SF₆ concentration



(f) Simulated SF₆ concentration

Figure 4. Comparison of the air velocity, air temperature, and SF₆ concentration distributions with the corresponding experimental data in the cross-section of the cabin through the fourth row.

4. Results

This investigation used the validated CFD model to study SARS-CoV-2 transmission in airliner cabins with the four different seat configurations for economy-class cabins shown in Figure 1. The thermo-fluid boundary conditions are provided in Table 1.

4.1 Airflow patterns and air temperature distributions in the cabins

Figure 5 depicts the airflow patterns and air temperature distributions in the cross-section through the passenger heads in the middle row (row 3) of the cabin mockups. The airflow

patterns on those airplanes were indeed completely mixing as designed. The mixing was driven by the overhead jets. The airflows contained two large eddies in the cross sections. The eddy was clockwise on the left side of each cabin and counter-clockwise on the right side, for all the cabins except the one with the 2-3-2 seat configuration. This was because the jets for the 2-3-2 seat configuration supplied air from the opposite directions. Nevertheless, the airflow seemed to be well mixed.

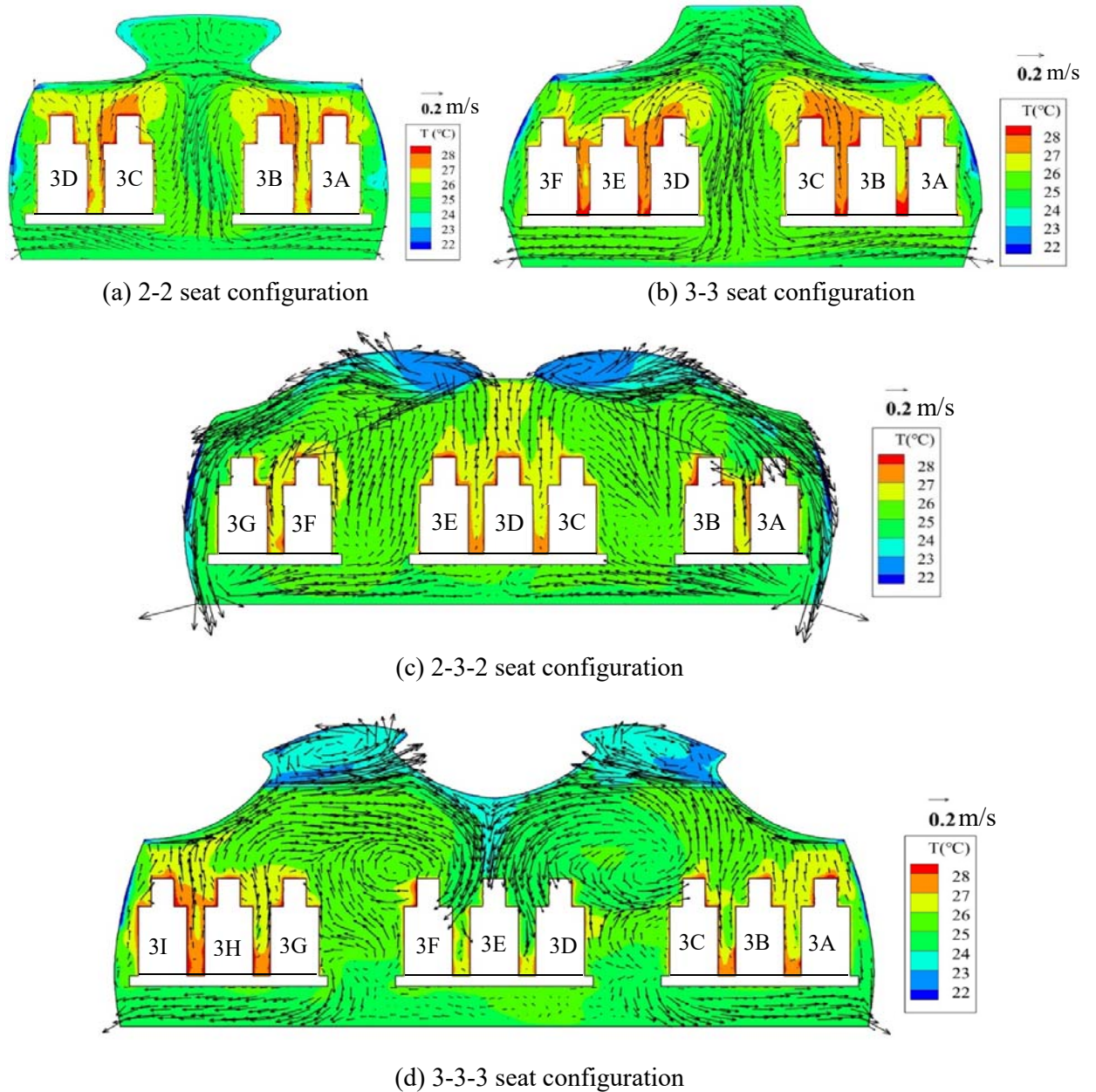


Figure 5. The airflow patterns and air temperature distributions in the cross-section through row 3 in the five-row cabin mockups.

Due to the complete mixing conditions, the air temperature distributions in the cabins were rather uniform. The cold air supply formed a low temperature near the supply region, while the

thermal plumes generated by the passengers led to a higher air temperature above the head regions and the areas around the bodies. The uniform air temperature distributions were designed to meet the thermal comfort requirements of the passengers.

Since limited space is available for this paper, Figure 6 presents only the airflow and air temperature distributions in the mid-longitudinal direction for the cabin mockup with the 2-3-2 seat configuration. Such aircraft were designed to have balanced air supply and air return for each row, and longitudinal airflow is supposed to be zero. However, we did observe moderate flow in the longitudinal direction. For the mockup with the 2-3-2 seat configuration, there was backward flow in the upper part of the mid-section in the cabins as shown in Figure 5, and forward flow on both sides near the walls. For the rest of the mockups, we found that the trends were reversed. Liu et al. [28] conducted airflow measurements in an MD-82 aircraft cabin. The experiment found also longitudinal flow. The longitudinal flow could be unstable that was caused by similar downward initial forces from the air supply and upward buoyancy forces from the thermal plums of the passengers. Again, the air temperature distributions along the longitudinal sections were rather uniform, while thermal plumes generated by the passengers were visible.

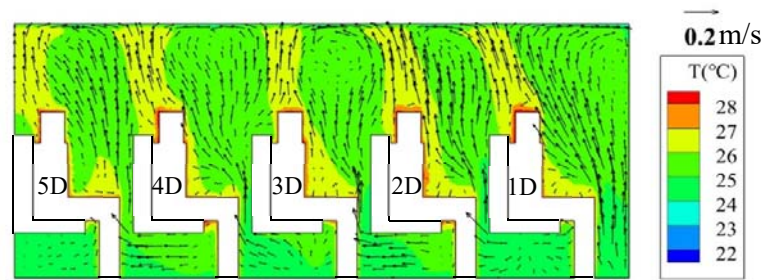
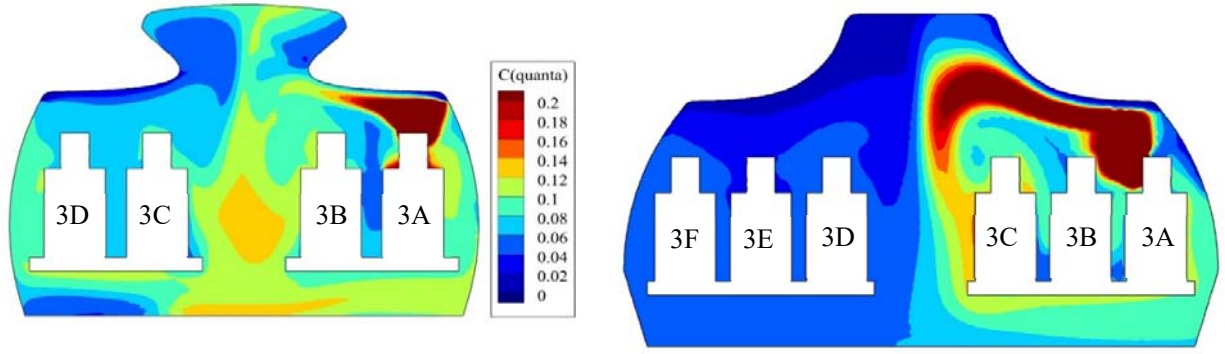


Figure 6. The airflow patterns and air temperature distributions in the mid-longitudinal section for the mockup with 2-3-2 seat configuration.

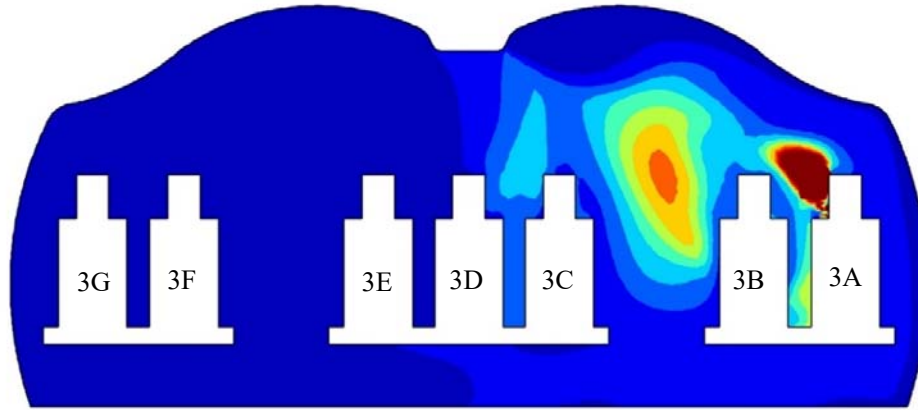
4.2 SARS-CoV-2 quanta distributions in the cabins

Figure 7 displays the SARS-CoV-2 quanta concentration distributions in the cross sections with an index patient sitting in seat 3A. The figure shows that, when the cabin was small, such as the 2-2 and 3-3 configurations, the virus was likely to be transmitted to the other side of the cabin in a cross section. For large cabins, the virus would be locked on the side of the cabin with the index patient. Although the air temperature distributions created by the environmental control systems were uniform in the cabins, the SARS-CoV-2 quanta distributions were not uniform. The air temperature distributions were the results of heat transfer from different surfaces and the jet flow. The temperature differences were not very high, as the lowest temperature was 20.7 °C from the jets and the highest temperature was 30.5 °C from the passenger head surfaces. However, the SARS-CoV-2 was only generated by the index patient, at a very high concentration of 66.7 quanta/m³ from the air breathed out by the patient. There was no other SARS-CoV-2 in the cabin, including the cleaning air supply. Although the mixing air supply system brought the virus to different places in the cabin, the SARS-CoV-2 quanta concentration was not uniform. The symmetric air supply prevented SARS-CoV-2 from being transferred to the other side of the cabins.

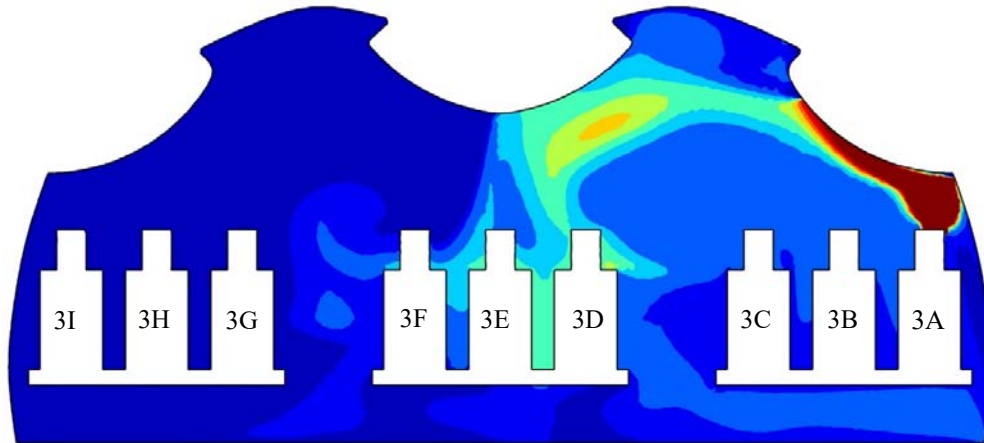


(a) 2-2 seat configuration

(b) 3-3 seat configuration



(c) 2-3-2 seat configuration



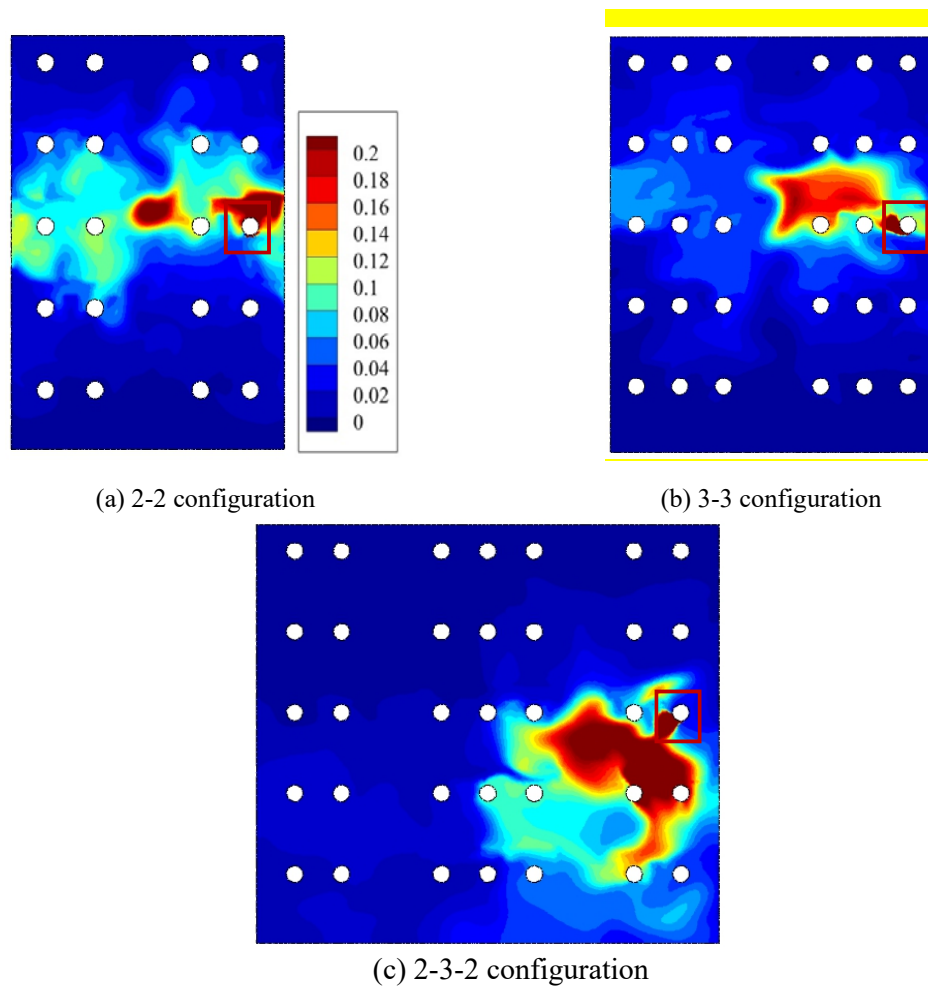
(d) 3-3-3 seat configuration

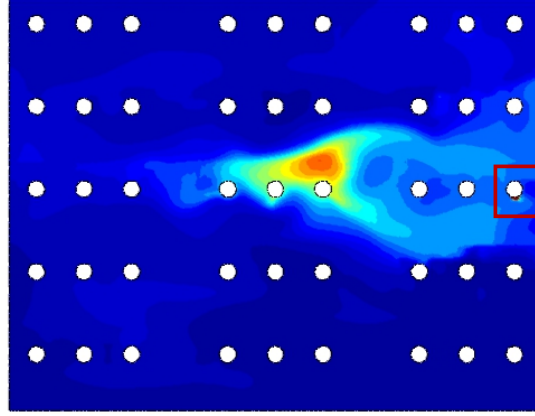
Figure 7. The SARS-CoV-2 quanta concentration distributions on the cross section through row 3 in the five-row cabin mockups assuming an index patient in Seat 3A.

Our simulated airflow patterns were rather symmetrical. Thus, the quanta could not be easily transferred from one side of the cabin to another. As a reviewer of this paper correctly pointed out: “The accuracy of the flow field simulation is crucial, as it mainly concerns the flow field.

The flow field in an aircraft is unstable and periodic.” In reality, the boundary conditions are not as symmetric as the simulated ones. Thus, the transfer of quanta from one side of the cabins to another side is likely.

Figure 8 illustrates the SARS-CoV-2 quanta concentration distributions at breathing level in the cabin mockups. The SARS-CoV-2 sources were the index patients in seat 3A, enclosed by the red square in the figure. In general, the SARS-CoV-2 quanta concentration was the highest in row 3. The 2-2, 3-3, and 3-3-3 configurations exhibited a slightly higher concentration in row 4 than that in row 2 because the airflows in those cabin mockups were moving backwards on the upper part of the index patient. However, the 2-3-2 configuration shows a much higher virus concentration in row 2 than in row 4 due to the forward airflow on the upper part of the index patient. During our study, we found that it was impossible to know in advance if the airflow on the upper part of a passenger would be forward to backward. The direction was very sensitive to the thermo-fluid boundary conditions. As the flows were unstable and periodic and actual boundary conditions were not symmetric, the actual quanta distributions for the cabins can be very different from the ones shown here. The results should be interpreted as a special case for each cabin, not universal ones.





(d) 3-3-3 configuration

Figure 8. The SARS-CoV-2 quanta concentration distributions at breathing level in the five-row cabin mockups assuming an index patient in Seat 3A enclosed by the red square.

4.3 Infection probability in the cabins with a four-hour flight

By using Eq. (3) and assuming an index patient seated in different seats of row 3 in the cabin mockups, this investigation next calculated the infection probability of fellow passengers who may be infected during a four-hour flight.

Figure 9 depicts the infection probability in the five-row cabin mockup with the 2-2 configuration. The infection rate was calculated from quanta concentration by using Eq. (3). For a specific passenger, the quanta concentration was the averaged value of a volume of 0.3 m x 0.3 m x 0.3 m in front of the passenger nose region. The average infection probability with the index patient in 3A was 3.2%, and with the index patient in 3B it was 3.4%. The index seat position did make a slight difference in the average infection rate. Since the cabin is symmetric along the aisle, one can easily use mirror results for the cases in which the index patient is in seats C and D. The overall average infection rate for the entire five-row cabin with the index patient in different positions was 3.4% for the four-hour flight. This percentage may not seem very high, but the infection probability for the passengers seated in the same row or in close proximity to the index patient could be around 10%. This is very high and seems to be in good agreement with infections reported by Hoehl et al. [2] in the early days of the COVID-19 pandemic.

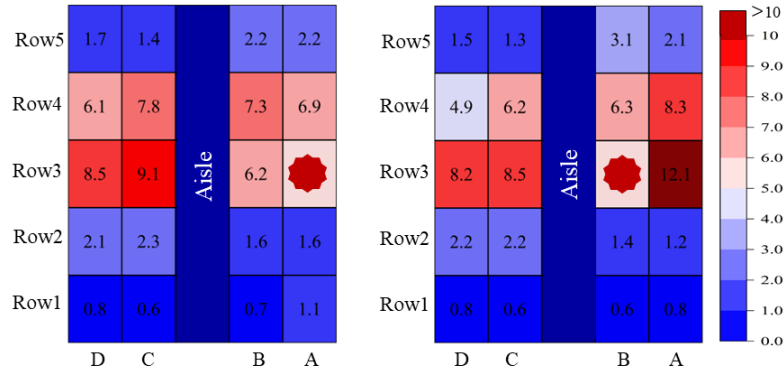
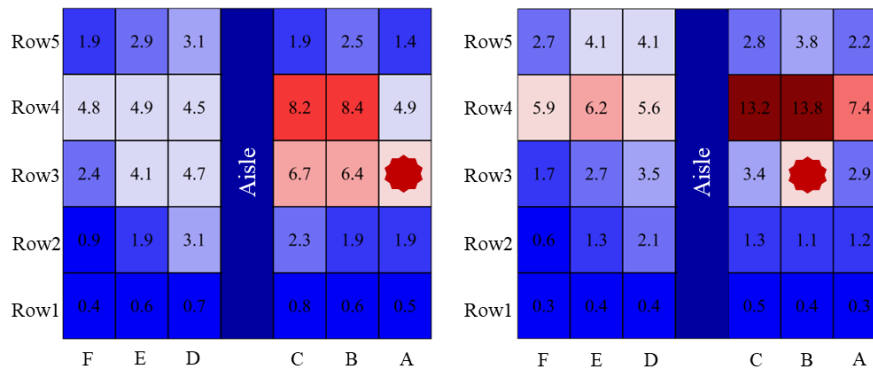


Figure 9. Infection probability (in %) in the cabin mockup with 2-2 configuration when an index patient is seated in 3A (left) and 3B (right).

Figure 10 shows the infection probability for the cabin mockup with the 3-3 seat configuration when the index patient is seated in 3A, 3B, and 3C, respectively. Very similar to the 2-2 seat configuration, the index patient position had an impact on the average infection rate among the passengers in the five rows. Our calculations found the infection probabilities for the five rows to be 2.1%, 2.1%, and 2.6%, respectively, when the index patient was seated in 3A, 3B, and 3C. The average infection probability for the three scenarios was 2.2%. This percentage was lower than that for the 2-2 configuration. However, this result should not be interpreted to mean that the 3-3 configuration was better than the 2-2 configuration. Because the 2-2 configuration was smaller, five rows contained only 20 passengers, whereas the 3-3 configuration had 30 passengers. To better compare the different types of aircraft, this investigation also compared the infection risk for the passengers in close proximity to the index patient, as described in the next section.



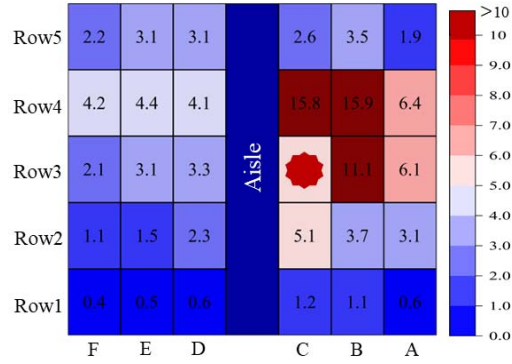


Figure 10. Infection probability (in %) in the cabin mockup with 3-3 configuration when the index patient is seated in 3A, 3B, and 3C, respectively. The color scale is the same as that in Figure 9.

The two figures in the Appendix of this paper illustrate the infection probability for the cabin mockups with 2-3-2 and 3-3-3 seat configurations. Similarly, the index patient was assumed to be in different seat position in row 3. The conclusions we drew from Figures 9 and 10 can be applied to the two large cabin mockups. Namely, different seat locations for the index patient would lead to different infection probabilities. The infection probabilities for the five rows of the cabin mockup with the 2-3-2 configuration were found to be 2.1%, 2.0%, 1.7% and 1.7%, respectively, when the index patient was seated in 3A, 3B, 3C and 3D. For the cabin mockup with the 3-3-3 configuration, the infection probabilities changed to 1.4%, 1.5%, 1.5%, 1.6%, and 1.3%, respectively, when the index patient was seated in 3A, 3B, 3C, 3D, and 3E. There was no clear trend in regard to which seat was better or worse. Even if we could identify such a trend, it might not be feasible to place an index patient in such a seat. The larger the cabin was, the lower the average infection probability was. The average probabilities were 3.3%, 2.2%, 1.9%, and 1.5%, respectively, for the 2-2, 3-3, 2-3-2, and 3-3-3 configurations. However, the average infection probability is not a good measure for assessing which cabin size was the best or the worst. This is because a large airplane has a large space, one index patient who infected same number of fellow passengers would have a lower average infection probability than that of a small airplane.

4.4 Assessment of infection probability in different types of cabin mockups

The results shown in the previous section indicated that the larger the cabin, the lower the COVID quanta concentration. The results are obvious because the source was fixed while the ventilation rate increased with cabin size. The average infection probability is not a good measure for evaluation of the cabin environment.

To be objective, this investigation averaged the infection probability for all the passengers sitting close to the index patient, namely, the passenger on the left, on the right, immediately in front of, and immediately behind the index patient. Table 2 shows the average infection probabilities for these peripheral passengers. The results illustrate that the infection probability

for the peripheral passengers depends on the index patient's position. The difference in the infection risk could be as high as three times when the index patient sits in different seats.

Table 2. The average infection probability for the peripheral passengers around the index patient in the cabins with different seat configurations (%)

Index patient's seat	3E	3D	3C	3B	3A	Average for all seats
2-2 configuration	NA	NA	NA	3.4	3.2	3.3
3-3 configuration	NA	NA	2.6	2.1	2.1	2.2
2-3-2 configuration	NA	1.7	1.7	2.0	2.1	1.9
3-3-3 configuration	1.3	1.6	1.5	1.5	1.4	1.5

We calculated the average infection probabilities for the peripheral passengers when the index patient was sitting in different seats. These average probabilities were 6.0%, 6.2%, 6.1%, and 4.6%, respectively, for the 2-2, 3-3, 2-3-2, and 3-3-3 seat configurations. The difference among the first three cabin types was statistically insignificant. The average infection probability for the 3-3-3 seat configuration was much lower than that for the other cabins. The airflow pattern would bring the virus from seat E to the flow level and exhaust it through the lower side wall. When the index patient was in seat A, the airflow pattern would lock the virus in an area above the patient. Thus, the airflow pattern can make a significant contribution to the infection probability. This finding was confirmed in a study conducted by Cao et al. [18].

In addition, it might not be fair to compare cabins with different seat configurations under the same flight duration. According to data from Flightstats (<https://www.flightstats.com/v2/>), the average flight times for the 2-2, 3-3, 2-3-3, and 3-3-3 seat configurations are 1.19 hours, 2.93 hours, 5.45 hours, and 9.51 hours, respectively, as depicted in Figure 11.

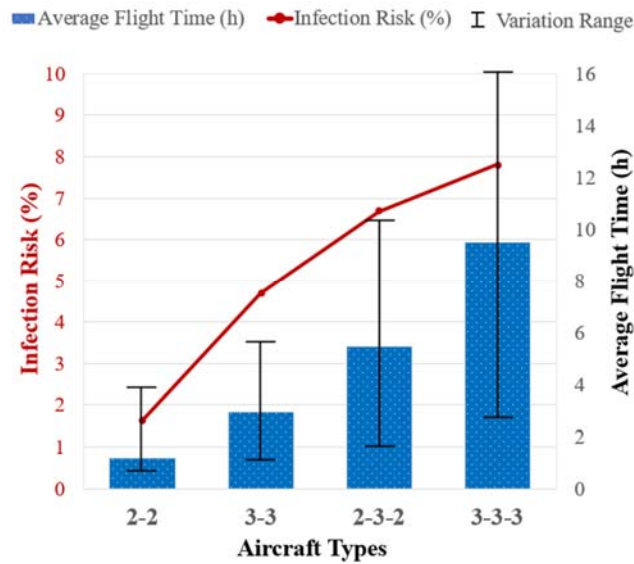


Figure 11. Infection probability for the peripheral passengers around the index patient in different cabin mockups with different flying times. The bars represent the flight time variation.

Figure 11 also shows the average infection probability for the peripheral passengers around the index patient in each type of aircraft cabin under different flight durations with the use of data from Flightstats. The longer a flight was, the higher the infection probability was. However, the risk was not proportional to time, because the infection probability was not the same among the cabin types. For a long-haul flight, the probability of becoming infected would be as high as 8% for a passenger sitting next to the index patient.

5. Discussion

The simulated results were not in perfect agreement with the experimental data, although the authors took every possible measure to simulate the case with experimental data carefully. As the cabin used for the experiment had a very complex geometry and complex thermo-fluid boundary conditions, the thermo-fluid boundary conditions were very difficult to control. The experimental instruments were also not free from errors. On the other hand, the turbulence model, the numerical technique, and many of the simulation parameters used approximations. The errors in the numerical aspects could be greater than the experimental errors. However, for the purpose of this study, the accuracy of the simulation results is acceptable, and the results reported on this paper are reliable.

The airflow patterns in the cabin mockups were very complex. Han et al. [46] studied the vortex structure of airflow in a 28-row aircraft cabin. They found an asymmetrical phenomenon in the instantaneous airflow field, instability on the longitudinal scale, and a large number of vortex structures generated in the collision zones. In the present study, the results presented for each type of aircraft cabin should be interpreted as a specific scenario. This investigation did not conduct additional simulations to ensure that the results were typical. This study also assumed fully occupied cabins, which is generally true in today's flight operations. It would be worthwhile to evaluate cases in which not all seats are occupied.

The simulations assumed that no passengers in the cabins wore masks and that the SARS-CoV-2 was highly toxic as in the early days of the pandemic, rather than current Omicron variant. Mask wearing would be beneficial in the cabin environment [5]. Furthermore, the variants of SARS-CoV-2 have become less toxic. Therefore, the infection probability for a passenger sitting next to an index patient would be far less than 8% during a long-haul flight. However, this study aims for the prevention of future pandemics of airborne diseases. The recent history has told us that such diseases could occur every a few years, such as SARS in 2003, H1N1 swine flu in 2009, and COVID-19. It is also very unlikely that passengers will wear masks in the beginning of such a pandemic.

6. Conclusions

This investigation used a validated CFD program and the Wells-Riley equation to determine infection probabilities for passengers during a flight. The cabins studied were economy-class with 2-2, 3-3, 2-3-2, and 3-3-3 seat configurations. Due to limitations in computing power, we studied only a five-row section of each cabin and assumed that one of the passengers was the index patient. The study led to the following conclusions:

With the modern aircraft cabin design, the airflow pattern in the cabin was generally well mixed. The air temperature distribution was rather uniform. However, the virus source was a point source that released the virus only in a specific location; the well-mixed ventilation system could not mix the virus thoroughly with the cabin air. In addition, due to the symmetric cabin design, virus from one side of the cabin might not be transferred easily to the other side of the cabin in a cross section. This was particularly true for larger aircraft cabins.

The infection probability depended on where the index patient was seated. There were no clear patterns in regard to which seat would cause a lower/higher infection risk than the other seats. The difference in the infection risk could be as high as three times when the index patient sits in different seats. Although the size of the cabins studied varied considerably, the average infection probabilities were similar, with the exception of the 3-3-3 seat configuration. The reason for the exception was that the airflow pattern in this configuration could bring the virus to the lower part of the cabin and exhaust it through the outlet, or could restrict the dispersion of the virus.

This investigation found that flight time was the most important factor in the infection probability. Without mask wearing among the passengers during a long-haul flight of around 10 hours in a twin-aisle, 3-3-3 seat cabin, the infection probability could have been around 8% for passengers sitting in close proximity to an index patient in the early days of the pandemic when the virus was very toxic.

CRedit authorship contribution statement

Feng Wang: Writing – original draft, Methodology, Investigation. **Tengfei (Tim) Zhang:** Writing – review & editing, Methodology, Conceptualization. **Ruoyu You:** Writing – review & editing, Methodology, Funding acquisition, Conceptualization. **Qingyan Chen:** Writing – review & editing, Supervision, Project administration.

Acknowledgements

This work was supported by the Early Career Scheme (Grant No. 25210419) of Research Grants Council of Hong Kong SAR, China.

References

- [1] S.H. Bae, H. Shin, H.Y. Koo, S.W. Lee, J.M. Yang, D.K. Yon, Asymptomatic transmission of SARS-CoV-2 on evacuation flight, *Emerg. Infect. Dis.* 26 (11) (2020) 2705.
- [2] S. Hoehl, O. Karaca, N. Kohmer, S. Westhaus, J. Graf, U. Goetsch, S. Ciesek, Assessment of SARS-CoV-2 transmission on an international flight and among a tourist group, *JAMA Netw. Open* 3 (8) (2020), e2018044 e2018044.
- [3] T. Toyokawa, T. Shimada, T. Hayamizu, T. Sekizuka, Y. Zukeyama, M. Yasuda, Y. Nakamura, S. Okano, J. Kudaka, T. Kakita, M. Kuroda, Transmission of SARS-CoV-2 during a 2-h domestic flight to okinawa, Japan, march 2020, *Influenza Respiratory Virus.* 16 (1) (2022) 63–71.

- [4] T. Swadi, J.L. Geoghegan, T. Devine, C. McElnay, J. Sherwood, P. Shoemack, X. Ren, M. Storey, S. Jefferies, E. Smit, J. Hadfield, Genomic evidence of in-flight transmission of SARS-CoV-2 despite predeparture testing, *Emerg. Infect. Dis.* 27 (3) (2021) 687.
- [5] F. Wang, R. You, T. Zhang, Q. Chen, Recent progress on studies of airborne infectious disease transmission, air quality, and thermal comfort in the airliner cabin air environment, *Indoor Air* 32 (4) (2022), e13032.
- [6] J.A. Pavlik, I.G. Ludden, S.H. Jacobson, E.C. Sewell, Airplane seating assignment problem, *Serv. Sci.* 13 (1) (2021) 1–18.
- [7] P.J. Edelson, Patterns of measles transmission among airplane travelers, *Trav. Med. Infect. Dis.* 10 (5–6) (2012) 230–235.
- [8] M.A. Miller, S. Valway, I.M. Onorato, Tuberculosis risk after exposure on airplanes, *Tuber. Lung Dis.* 77 (5) (1996) 414–419.
- [9] WHO. <https://www.who.int/westernpacific/emergencies/covid-19/information/physical-distancing>, 2022.
- [10] CDC. <https://www.cdc.gov/coronavirus/2019-ncov/prevent-getting-sick/prevention.html>, 2022.
- [11] N.C. Khanh, P.Q. Thai, H.L. Quach, N.A.H. Thi, P.C. Dinh, T.N. Duong, L.T.Q. Mai, N.D. Nghia, T.A. Tu, L.N. Quang, Q.T. Dai, Transmission of SARS-CoV 2 during long-haul flight, *Emerg. Infect. Dis.* 26 (11) (2020) 2617.
- [12] A. Mangili, M.A. Gendreau, Transmission of infectious diseases during commercial air travel, *Lancet* 365 (9463) (2005) 989–996.
- [13] T. Mizuno, M.J. Warfield, Development of Three-Dimensional Thermal Airflow Analysis Computer Program and Verification Test, vol. 98, ASHRAE TRANS, ASHRAE, ATLANTA, GA(USA), 1992, pp. 329–338, 1992.
- [14] C.H. Lin, K.H. Dunn, R.H. Horstman, J.L. Topmiller, M.F. Ahlers, J.S. Bennett, L. M. Sedgwick, S. Wirogo, Numerical simulation of airflow and airborne pathogen transport in aircraft cabins–Part II: numerical simulation of airborne pathogen transport, *Build. Eng.* 111 (1) (2005).
- [15] S.M. Kinahan, D.B. Silcott, B.E. Silcott, et al., Aerosol tracer testing in Boeing 767 and 777 aircraft to simulate exposure potential of infectious aerosol such as SARS-CoV-2, *PLoS One* 16 (12) (2021), e0246916.
- [16] W. Yan, Y. Zhang, Y. Sun, et al., Experimental and CFD study of unsteady airborne pollutant transport within an aircraft cabin mock-up, *Build. Environ.* 44 (1) (2009) 34–43.
- [17] R. You, W. Liu, J. Chen, C.H. Lin, D. Wei, Q. Chen, Predicting airflow distribution and contaminant transport in aircraft cabins with a simplified gasper model, *J. Build Performance Simul.* 9 (6) (2016) 699–708.
- [18] Q. Cao, M. Liu, X. Li, C.H. Lin, D. Wei, S. Ji, T.T. Zhang, Q. Chen, Influencing Factors in the Simulation of Airflow and Particle Transportation in Aircraft Cabins by CFD, vol. 207, *Building and Environment*, 2022, 108413.
- [19] Y. Yan, X. Li, L. Yang, P. Yan, J. Tu, Evaluation of cough-jet effects on the transport characteristics of respiratory-induced contaminants in airline passengers’ local environments, *Build. Environ.* 183 (2020), 107206.
- [20] R. You, C.H. Lin, D. Wei, Q. Chen, Evaluating the commercial airliner cabin environment with different air distribution systems, *Indoor Air* 29 (5) (2019) 840–853.

- [21] V.S. Hertzberg, H. Weiss, On the 2-row rule for infectious disease transmission on aircraft, *Annal Global Health*. 82 (5) (2016) 819–823.
- [22] J.K. Gupta, C.H. Lin, Q. Chen, Risk assessment of airborne infectious diseases in aircraft cabins, *Indoor Air* 22 (5) (2012) 388–395.
- [23] W. Wang, F. Wang, D. Lai, Q. Chen, Evaluation of SARS-COV-2 transmission and infection in airliner cabins, *Indoor Air* (2022), <https://doi.org/10.1111/ina.12979>.
- [24] R. Horstman, H. Rahai, A risk assessment of an airborne disease inside the cabin of a passenger airplane, in: *SAE International Journal of Advances and Current Practices in Mobility*, 3, 2021, pp. 1263–1271, 2021-01-0036.
- [25] S. Yin, G.N. Sze-To, C.Y. Chao, Retrospective Analysis of Multi-Drug Resistant Tuberculosis Outbreak during a Flight Using Computational Fluid Dynamics and Infection Risk Assessment, vol. 47, *Building and Environment*, 2012, pp. 50–57.
- [26] Y. Yan, X. Li, Y. Shang, J. Tu, Evaluation of airborne disease infection risks in an airliner cabin using the Lagrangian-based Wells-Riley approach, *Build. Environ.* 121 (2017) 79–92.
- [27] M. Liu, J. Liu, Q. Cao, X. Li, S. Liu, S. Ji, C.H. Lin, D. Wei, X. Shen, Z. Long, Q. Chen, Evaluation of Different Air Distribution Systems in a Commercial Airliner Cabin in Terms of Comfort and COVID-19 Infection Risk, vol. 208, *Building and Environment*, 2022, 108590.
- [28] W. Liu, J. Wen, J. Chao, W. Yin, C. Shen, D. Lai, C.H. Lin, J. Liu, H. Sun, Q. Chen, Accurate and high-resolution boundary conditions and flow fields in the first-class cabin of an MD-82 commercial airliner, *Atmos. Environ.* 56 (2012) 33–44.
- [29] V. Yakhot, S.A. Orszag, Renormalization group analysis of turbulence. I. Basic theory, *J. Sci. Comput.* 1 (1) (1986) 3–51.
- [30] Z. Zhang, W. Zhang, Z.J. Zhai, Q.Y. Chen, Evaluation of various turbulence models in predicting airflow and turbulence in enclosed environments by CFD: Part 2—comparison with experimental data from literature, *HVAC R Res.* 13 (6) (2007) 871–886.
- [31] D.D. Gray, A. Giorgini, The validity of the Boussinesq approximation for liquids and gases, *Int. J. Heat Mass Tran.* 19 (5) (1976) 545–551.
- [32] ANSYS FLUENT, 14.5, User's and Theory Guide, ANSYS, Inc, Canonsburg, Pennsylvania, USA, 2014.
- [33] J.M. Beneke, B.W. Jones, M. Hosni, Fine particle dispersion in a commercial aircraft cabin, *HVAC R Res.* 17 (1) (2011) 107–117.
- [34] W.L. Dietrich, J.S. Bennett, B.W. Jones, M.H. Hosni, Laboratory modeling of SARS-CoV-2 exposure reduction through physically distanced seating in aircraft cabins using bacteriophage aerosol—november 2020, *MMWR (Morb. Mortal. Wkly. Rep.)* 70 (16) (2021) 595.
- [35] B. Li, R. Duan, J. Li, Y. Huang, H. Yin, C.H. Lin, D. Wei, X. Shen, J. Liu, Q. Chen, Experimental studies of thermal environment and contaminant transport in a commercial aircraft cabin with gaspers on, *Indoor Air* 26 (5) (2016) 806–819.
- [36] W.F. Wells, *Airborne Contagion and Air Hygiene*, Cambridge University Press, Cambridge MA, 1955, pp. 117–122.
- [37] E.C. Riley, G. Murphy, R.L. Riley, Airborne spread of measles in a suburban elementary school, *Am. J. Epidemiol.* 107 (5) (1978) 421–432.

- [38] H. Dai, B. Zhao, Association of the infection probability of COVID-19 with ventilation rates in confined spaces, in: *In Building Simulation*, vol. 13, Tsinghua University Press, 2020, December, pp. 1321–1327, 6.
- [39] F. Li, J. Liu, J. Pei, C.H. Lin, Q. Chen, Experimental study of gaseous and particulate contaminants distribution in an aircraft cabin, *Atmos. Environ.* 85 (2014) 223–233.
- [40] Q. Chen, J. Srebric, A procedure for verification, validation, and reporting of indoor environment CFD analyses, *HVAC R Res.* 8 (2) (2002) 201–216.
- [41] M. Li, B. Zhao, J. Tu, Y. Yan, Study on the carbon dioxide lockup phenomenon in aircraft cabin by computational fluid dynamics, *Build. Simulat.* 8 (2015) 431–441.
- [42] F.A. Guevara Luna, M.A. Guevara Luna, L.C. Belalcazar Ceron, CFD modeling and validation of tracer gas dispersion to evaluate self-pollution in school buses, *Asia J. Atmosphere. Environ.* 13 (1) (2019) 1–10.
- [43] T. Zhang, P. Li, Y. Zhao, S. Wang, Various air distribution modes on commercial airplanes—Part 2: computational fluid dynamics modeling and validation, *HVAC R Res.* 19 (5) (2013) 457–470.
- [44] C.A. Mboreha, S. Jianhong, W. Yan, S. Zhi, Airflow and contaminant transport in innovative personalized ventilation systems for aircraft cabins: a numerical study, *Sci. Technol. Build Environ.* 28 (4) (2022) 557–574.
- [45] T. Zhang, P. Li, Y. Zhao, S. Wang, Various air distribution modes on commercial airplanes. Part 1: experimental measurement, *HVAC R Res.* 19 (3) (2013) 268–282.
- [46] Y. Han, Y. Zhang, Y. Gao, X. Hu, Z. Guo, Vortex structure of longitudinal scale flow in a 28-row aircraft cabin, *Build. Environ.* 222 (2022), 109362.

Appendix

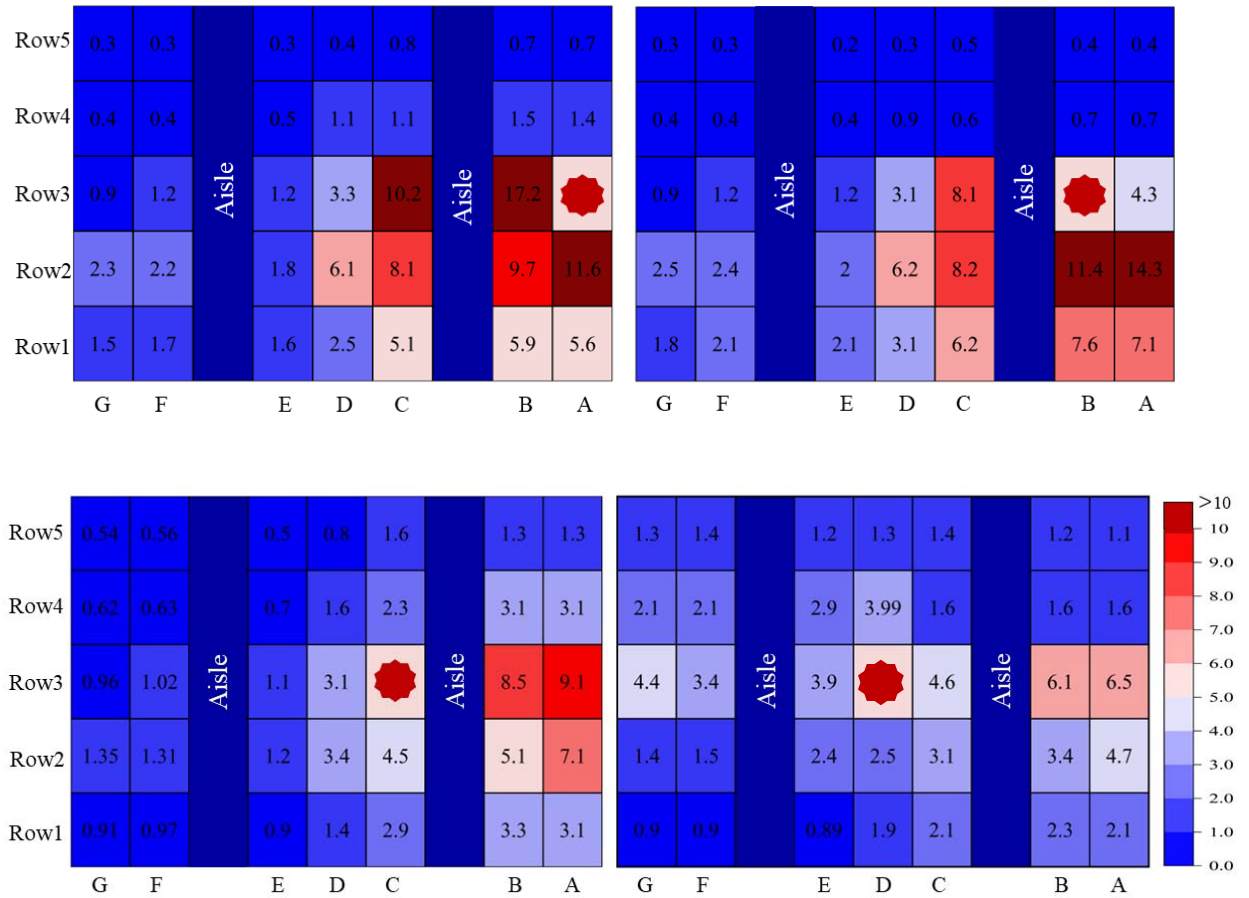





Figure A1. Infection probability in the cabin mockup with 2-3-2 seat configuration when the index patient is seated in 3A, 3B, 3C, and 3D, respectively. The color scale is shown in Figure A2.

Row5	1.3	1.2	1.2	Aisle	1.1	1.1	1.5	Aisle	2.2	2.9	2.3
Row4	2.1	1.7	1.5		1.7	0.9	2.8		3.6	4.3	4.9
Row3	1.7	1.6	1.6		2.6	4.1	6.4		5.5	5.7	
Row2	1.1	1.7	1.8		1.4	0.6	0.8		0.8	0.7	0.8
Row1	0.8	0.9	1.1		0.9	0.6	0.6		0.6	0.6	0.6
	I	H	G		F	E	D		C	B	A

Row5	0.9	0.8	0.8	Aisle	0.8	0.7	1.1	Aisle	1.4	1.9	1.5
Row4	1.3	1.2	1.1		1.2	0.7	1.6		2.1	2.9	3.6
Row3	1.5	1.3	1.4		1.8	4.5	13.9		9.1		11.7
Row2	0.9	1.3	1.4		1.1	0.6	1.3		1.6	1.3	1.4
Row1	0.8	0.8	0.9		0.8	0.8	1.2		1.1	1.1	1.1
	I	H	G		F	E	D		C	B	A

Row5	1.3	1.2	1.3	Aisle	1.2	1.1	1.1	Aisle	1.5	1.9	1.5
Row4	2.1	1.8	1.5		1.7	1.1	2.2		2.1	2.6	3.3
Row3	1.9	1.8	1.8		2.8	6.9	12.6			9.4	8.6
Row2	1.1	1.8	1.9		1.5	0.7	1.1		1.2	1.1	1.2
Row1	0.9	1.1	1.1		1.1	0.9	0.9		0.9	0.9	0.9
	I	H	G		F	E	D		C	B	A

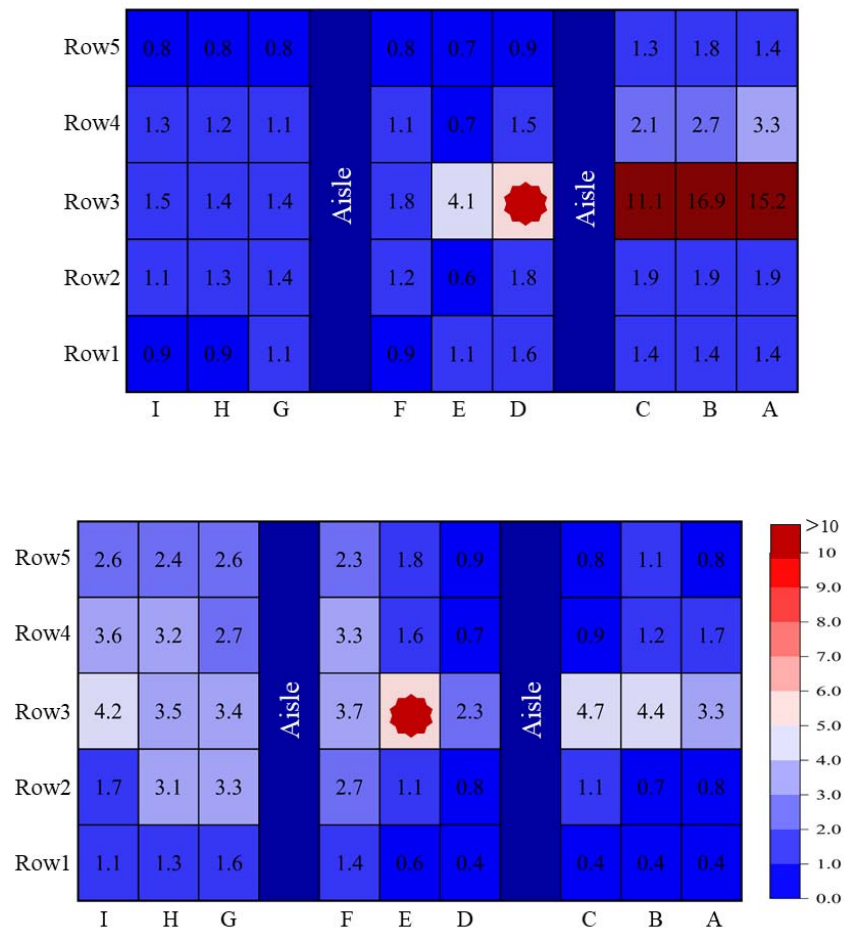


Figure A2. Infection probability in the cabin mockup with 3-3-3 seat configuration when the index patient is seated in 3A, 3B, 3C, 3D, and 3E, respectively.